Progress In Electromagnetics Research C, Vol. 95, 251–264, 2019

The Fractional Derivative Approach for Diffraction Problems: Plane Wave Diffraction by Two Strips with Fractional Boundary Conditions

Vasil Tabatadze[1, 2, *], Kamil Karaçuha[1], and Eldar I. Veliyev[1, 3]

Abstract—In this article, a solution of the plane wave diffraction problem by two axisymmetric strips with different dimensions is considered. Fractional boundary conditions are required on the surface of each strip. Several cases of strip's dimension, configurations, and fractional orders are considered, and numerical results are obtained. The near electric field distribution, Total Radar Cross Section frequency characteristics, and the Poynting vector distribution in the vicinity of these strips are calculated and illustrated. For the fractional order 0.5, the solution is found analytically.

1. INTRODUCTION

In the last decades, the tools of the fractional calculus which use fractional operators have an increasing number of applications in physics and electrodynamics. The interest in fractional operators is related to the fact that fractional operators broaden the notion of the initial operator. If the initial operator is related to the description of some canonical cases, the fractional operators with non-integer order can describe a new problem with new properties. Therefore, fractional operators generalize the class of problems studied in different areas of the science [1–3].

Applications of fractional operators in electrodynamics were developed by Engheta and then, Veliev and Ivakhnychenko [1–5]. Engheta proposed a fractional paradigm which states that if the function and its first derivative describe two canonical states of the electromagnetic field, then the fractional derivative describes an intermediate state of the field between the canonical states [1]. Veliev and Ivakhnychenko developed this idea further and considered the generalization of boundary conditions. In this article, there are introduced fractional boundary conditions (FBC) which correspond to intermediate boundary conditions between the perfect electric conductor and perfect magnetic conductor [6]. These boundary conditions describe a new material which was studied in the previous works [7–11]. In these works, electromagnetic scattering problems were considered such as the diffraction by one strip, two strips with the same length and a half-plane with fractional boundary condition where the theoretical part is formulated, and for one strip case, some numerical results are also obtained. Some other authors also have publications in this direction and made contributions in fractional calculus development in electrodynamics [12–15].

This study more deeply investigates the properties of such a new material which satisfies the fractional boundary condition. The theoretical description of electromagnetic plane wave scattering by the two strips with different dimensions is given in the theoretical section. After that, the total electric field distribution and Total Radar Cross Section (TRCS) are investigated and obtain numerical results. In the general case, the solution of the problem is reduced to a solution of a system of linear algebraic equations (SLAE) which can be obtained with a given accuracy. However, for the values of the fractional order (FO) $\alpha = 0.5$, the solution is obtained in an analytical form which is the advantage

Received 25 June 2019, Accepted 29 August 2019, Scheduled 16 September 2019

* Corresponding author: Vasil Tabatadze (vasilitabatadze@gmail.com).

[1] Informatics Institute of Istanbul Technical University, Maslak, Istanbul 34469, Turkey. [2] Tbilisi State University, 1 Chavchavadze Avenue, Tbilisi 0179, Georgia. [3] National University of 'Kharkiv Polytechnic Institute', Kharkiv 61000, Ukraine.

of the fractional derivative method (FDM) [7–9]. In results of the numerical simulation part, TRCS shows the presence of resonances which are associated with the excitation of quasi-self-oscillations of a double strip resonator.

The method represented in the paper is an efficient and new fundamental approach for diffraction problems because the method requires one integral equation and one current density for each strip, whereas by using impedance boundary condition, two current densities namely, electric and magnetic current densities, and two integral equations for each strip are needed [7].

2. THEORETICAL PART

In this problem, there are two axisymmetric strips with different widths and infinite length in z-axis located at $y = \pm l$ planes. The widths of the strips are $2a_1$ and $2a_2$, respectively. In Figure 1, the geometry of the problem is given.

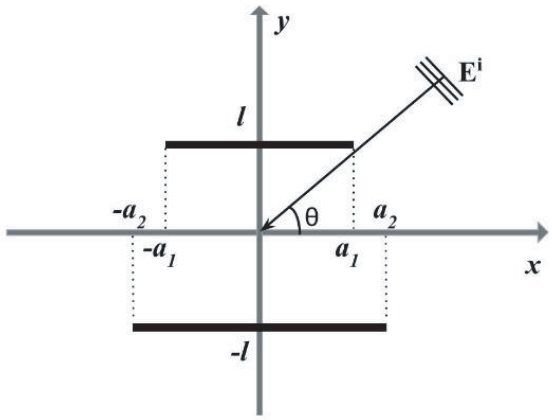

Figure 1. The geometry of the problem.

As an incident field, there is an E-polarized electromagnetic plane wave. The electric field has only a z component and can be written as $E_z^i = e^{-ik(x\cos\theta + y\sin\theta)}$ where $\mathbf{k}$ is the wavenumber, and $\boldsymbol{\theta}$ is the angle of incidence. A total electric field is given as $E_z = E_z^i + E_z^s$ where E_z^s stands for the total scattered electric field by both strips. The total electric field E_z should satisfy the fractional boundary condition (FBC) on each strip. The fractional boundary condition is given in Eq. (1).

$$D_{ky}^{\alpha} E_z(x,y) = 0, \quad y \to \pm l, \quad x \in (-a_i,\, a_i), \quad i = 1,2 \tag{1}$$

where α is a fractional order (FO); the fractional derivative is given in Eq. (1); D_{ky}^{α} is determined by the Riemann-Liouville equation [4, 5, 16] which has the form as Eq. (2).

$$D_y^{\alpha} f(y) = \frac{1}{\Gamma(1-\alpha)} \frac{d}{dy} \int_{-\infty}^{y} \frac{f(t)}{(y-t)^{\alpha}} dt, \tag{2}$$

where, $\Gamma(1-\alpha)$ is Gamma Function, and $\alpha \in (0,1)$.

When $\alpha = 0$, the boundary condition corresponds to the perfect electric conductor (PEC). When $\alpha = 1$, it stands for the perfect magnetic conductor (PMC). For FO between $0 < \alpha < 1$, FBC corresponds to the intermediate case between PEC and PMC. Previous studies show that when fractional order is in this range, the strip boundary corresponds to the material with a pure imaginary impedance which is called fractional impedance. The relation between the fractional order and fractional impedance is given with the following formula, $\eta_{\alpha} = -\frac{i}{\sin\theta} \tan\left(\frac{\pi}{2}\alpha\right)$ for any incidence angle [7, 8]. From this expression, it is easy to get the next formula $\alpha = \frac{1}{i\pi} \ln\left(\frac{1-\eta_{\alpha}\sin\theta}{1+\eta_{\alpha}\sin\theta}\right)$ [4, 7, 9].

The use of fractional boundary condition is advantageous because it needs only one integral equation to be solved, while in the case of ordinary impedance boundary condition, two integral equations must

be solved [8, 9]. In order to formulate the problem, first, time dependency and field expressions need to be defined. Here, throughout formulation, the time dependency is $e^{-i\omega t}$, and it is omitted everywhere.

The scattered electric field $E_z^s(xy)$ is the sum of two parts which are the scattered fields by the first and second strips, respectively. Total scattered electric field is $E_z^s(x,y) = E_z^{s1}(x,y) + E_z^{s2}(xy)$, and each part can be found by Eq. (3) [9].

$$E_z^{sj}(x,y) = \int_{-\infty}^{\infty} f_j^{1-\alpha}(x') G^{\alpha}(x-x', y_j)\, dx', \quad j=1,2, \quad y_1 = y-l, \quad y_2 = y+l, \tag{3}$$

where,

$$G^{\alpha}(x-x', y) = i\frac{1}{4\pi} D_{ky}^{\alpha} \int_{-\infty}^{\infty} e^{ik\left[q(x-x')+|y|\sqrt{1-q^2}\right]} (1-q^2)^{\frac{\alpha-1}{2}} d\alpha.$$

Here, $f^{1-\alpha}(x')$ is the fractional density of surface current on the strip. In Eq. (3), $j = 1, 2$ corresponds to the upper or lower strip, respectively, and $G^{\alpha}(x-x', y)$ is the fractional Green's function which is, in the two-dimensional case, $G^{\alpha}(x-x', y) = -\frac{i}{4} D_{ky}^{\alpha} H_0^{(1)}(k\sqrt{(x-x')^2+y^2})$ [5, 7, 8]. In the expression, $H_0^{(1)}(z)$ is the Hankel function of the first kind and zero order. Note that in Eq. (3), the plane wave expansion of Hankel function is used. Then, Eq. (4) is achieved by representing $f_j^{1-\alpha}(x')$ with its corresponding Fourier transform $F_j^{1-\alpha}(q)$ [9, 10].

$$E_z^{sj}(x, y_j) = -i\frac{e^{\pm i\frac{\pi}{2}\alpha}}{4\pi} \int_{-\infty}^{\infty} F_j^{1-\alpha}(q)\, e^{ik\left(xq+|y_j|\sqrt{1-q^2}\right)} \left(1-q^2\right)^{\frac{\alpha-1}{2}} dq \tag{4}$$

where $y_1 = y-l$, $y_2 = y+l$, $j = 1, 2$, and

$$\begin{aligned}
F_j^{1-\alpha}(q) &= \int_{-1}^{1} \tilde{f}_j{}^{1-\alpha}(\xi)\, e^{-i\varepsilon q\xi} d\xi, \\
\tilde{f}_j{}^{1-\alpha}(\xi) &= \frac{\varepsilon_j}{2\pi} \int_{-\infty}^{\infty} F_j^{1-\alpha}(q)\, e^{i\varepsilon_j q\xi} dq, \\
\tilde{f}_j{}^{1-\alpha}(\xi) &= a f_j^{1-\alpha}(\xi), \quad \epsilon_j = ka_j, \quad \xi = \frac{x}{a_j}.
\end{aligned}$$

Equations (3) and (4) are chosen so that the total electric field E_z satisfies Helmholtz equation, and also, the scattered electric field E_z^s satisfies Sommerfeld radiation condition at the infinity [7, 9].

After applying the FBC on the surface of each strip and multiplying both sides of the integral equation (4) by $\int_{-a_i}^{a_i} e^{-ikx\tau} dx$, the integral equation system is as Eq. (5) where the upper sign stands for $i = 1$, and, for the lower sign, $i = 2$ needs to be taken into account. Different signs in the exponent ($e^{\mp ikl\sin\theta}$) correspond to the upper and lower strips, respectively. Keep in mind that ($\pm i$), which comes from the fractional boundary condition, is given in Eq. (1). Here, (+) sign corresponds to the upper part of each strip, and (−) sign stands for the lower part of each strip.

$$\begin{aligned}
&\int_{-\infty}^{\infty} F_i^{1-\alpha}(q) \frac{\sin(ka_i(q-\tau))}{(q-\tau)} \left(1-q^2\right)^{\alpha-\frac{1}{2}} dq = -i4\pi (\pm i)^{\alpha} e^{\mp ikl\sin\theta} \sin^{\alpha}\theta \frac{\sin(ka_i(\tau+\cos\theta))}{(\tau+\cos\theta)} \\
&- \int_{-\infty}^{\infty} F_j^{1-\alpha}(q) \frac{\sin(ka_i(q-\tau))}{(q-\tau)} e^{ik2l\sqrt{1-q^2}} \left(1-q^2\right)^{\alpha-\frac{1}{2}} dq, \quad i,j=1,2, \quad i \neq j
\end{aligned} \tag{5}$$

In order to solve the set of integral equations (IE) in Eq. (5), the IE is reduced to the system of linear algebraic equation by presenting the unknown $\zeta_{n_i}^{\alpha}$ as series of the Gegenbauer polynomials given in Eq. (6) [9–11]. Here, the Gegenbauer polynomials series for the normalized current density are used with the weighting function $(1-\xi_i)^{\alpha-\frac{1}{2}}$ in order to satisfy well-known Meixner's edge condition [17].

$$\tilde{f}_i^{1-\alpha}(\xi_i) = (1-\xi_i)^{\alpha-\frac{1}{2}} \sum_{n=0}^{\infty} \zeta_{n_i}^{\alpha} \frac{C_n^{\alpha}(\xi_i)}{\alpha} \tag{6}$$

The corresponding Fourier transform is shown in Eq. (7) [9–11].

$$F_i^{1-\alpha}(q) = \frac{2\pi}{\Gamma(\alpha+1)} \sum_{n=0}^{\infty} (-i)^n \zeta_{n_i}^{\alpha} \beta_n^{\alpha} \frac{J_{n+\alpha}(\epsilon_i q)}{(2\epsilon_i q)^{\alpha}}, \tag{7}$$

where,

$$\epsilon_i = ka_i, \quad \beta_n^{\alpha} = \frac{\Gamma(n+2\alpha)}{\Gamma(n+1)}, \quad i = 1, 2.$$

The weighting function $(1-\xi_i)^{\alpha-\frac{1}{2}}$ in Eq. (6) is chosen so that it satisfies edge conditions [17]. After Eq. (7) is put in Eq. (5), then multiplied by $\frac{J_{k+\alpha}(\epsilon_1\tau)}{\tau^{\alpha}}$ and $\frac{J_{k+\alpha}(\epsilon_2\tau)}{\tau^{\alpha}}$ for corresponding integral equations $i = 1$ and $i = 2$, respectively, the overall result for the upper and lower strips is as Eq. (8). Note that IE in Eq. (5) is integrated with parameter τ between $(-\infty, \infty)$ in order to get Eq. (8).

$$\sum_{n=0}^{\infty} (-i)^n \zeta_{n_i}^{\alpha} \beta_n^{\alpha} C_{kn}^{\alpha(i,i)} + \left(\frac{\epsilon_i}{\epsilon_j}\right)^{\alpha} \sum_{n=0}^{\infty} (-i)^n \zeta_{n_j}^{\alpha} \beta_n^{\alpha} C_{kn}^{\alpha(i,j)} = \gamma_k^{i,\alpha}, \quad i,j = 1,2, \quad i \neq j \tag{8}$$

Here,

$$C_{kn}^{\alpha(i,i)} = \int_{-\infty}^{\infty} J_{n+\alpha}(\epsilon_i q) J_{k+\alpha}(\epsilon_i q) \frac{\left(1-q^2\right)^{\alpha-\frac{1}{2}}}{q^{2\alpha}} dq,$$

$$C_{kn}^{\alpha(i,j)} = \int_{-\infty}^{\infty} J_{n+\alpha}(\epsilon_j q) J_{k+\alpha}(\epsilon_i q) e^{ik2l\sqrt{1-q^2}} \frac{\left(1-q^2\right)^{\alpha-\frac{1}{2}}}{q^{2\alpha}} dq, \quad i \neq j,$$

$$\gamma_k^{i,\alpha} = -i2(\pm i)^{\alpha} (2\epsilon_i)^{\alpha} \Gamma(\alpha+1) e^{\mp ikl\sin\theta} \tan^{\alpha}\theta (-1)^k J_{k+\alpha}(\epsilon_i \cos\theta).$$

It can be shown that the system of linear algebraic equation (SLAE) (8) can be reduced to SLAE of the Fredholm type of the second kind [9]. Then, the coefficients $\zeta_{n_j}^{\alpha}$ can be found with any desired accuracy (within the machine precision) by using the truncation of SLAE (8). Note that, for the fractional order $\alpha = 0.5$, the solution can be found analytically [8, 9]. After applying the boundary condition for FO $\alpha = 0.5$, analytically, Fourier transform of the current density in the upper and lower strips can be found by using Eq. (5), and the result is given in Eq. (9).

$$F_i^{0.5}(\tau) = \frac{-i4e^{\frac{i\pi}{4}}\sqrt{\sin\theta}\left(\frac{\sin(ka_i(\tau+\cos\theta))}{(\tau+\cos\theta)} e^{\mp ikl\sin\theta} - \frac{\sin(ka_j(\tau+\cos\theta))}{(\tau+\cos\theta)} e^{\pm ikl\sin\theta} e^{ik2l\sqrt{1-\tau^2}}\right)}{\left[1 - e^{ik4l\sqrt{1-\tau^2}}\right]} \tag{9}$$

where $i, j = 1, 2$, $i \neq j$.

Having expression for $F_i^{1-\alpha}$ in Eq. (7) and $F_i^{0.5}$ in Eq. (9), the radiation pattern of the scattered field in the far zone can be found by using Eq. (10). Using the stationary phase method for $ka \to \infty$, the scattered electric field gets the next form:

$$E_z^s(x,y) = A(kr)\Phi^{\alpha}(\phi). \tag{10}$$

Here,

$$A(kr) = \sqrt{\frac{2}{\pi kr}} e^{ikr - \frac{i\pi}{4}}, \quad \text{and} \quad \Phi^{\alpha} = \Phi_1^{\alpha}(\phi) + \Phi_2^{\alpha}(\phi),$$

where,

$$\Phi_1^{\alpha}(\phi) = -\frac{i}{4} e^{\pm\frac{i\pi\alpha}{2}} F_1^{1-\alpha}(\cos\phi)(\sin^{\alpha}\phi) e^{-ikl\sin\phi},$$

$$\Phi_2^{\alpha}(\phi) = -\frac{i}{4} e^{\pm\frac{i\pi\alpha}{2}} F_2^{1-\alpha}(\cos\phi)(\sin^{\alpha}\phi) e^{+ikl\sin\phi}.$$

The upper sign is chosen for $\phi \in [0, \pi]$, and the lower sign is for $\phi \in [\pi, 2\pi]$ in Eq. (10) where ϕ is the observation angle. $A(kr)$ is the radial part, and $\Phi^{\alpha}(\phi)$ is the angular part of the scattered electric

field in the far zone. The radiation pattern (RP) $\Phi^{\alpha}(\phi)$ expression in Eq. (10) is used for Total Radar Cross Section calculation [18]. The definition of the Total Radar Cross Section is given in (11).

$$\sigma_t = \int_0^{2\pi} |\Phi^{\alpha}|^2 \, d\phi \tag{11}$$

As it has already been mentioned, the total electric field E_z has only a z-component, and the magnetic field has x and y components H_x and H_y, respectively. The Poynting vector S has x and y components and is calculated by using the formula in Eq. (12) [19].

$$S = \frac{1}{2}\mathrm{Re}\left[E \times H^*\right], \quad S_x = -\frac{1}{2}\mathrm{Re}\left[E_z H_y^*\right], \quad S_y = \frac{1}{2}\mathrm{Re}\left[E_z H_x^*\right] \tag{12}$$

Here, $(*)$ denotes the complex conjugate.

3. RESULTS OF NUMERICAL SIMULATIONS

Based on the described mathematical algorithm, the program package was created in MatLab, and several cases of strips dimension and fractional orders were considered. The near field distribution was calculated, and the Total Radar Cross Section dependence on the wavenumber was constructed. The results are given below.

First, the case in which the strips have the same length is considered. Figure 2 shows the family of graphs depending on different fractional orders. Total Radar Cross Section (σ_T) has dependency on $\epsilon = ka$ for different Fractional orders ($\alpha = 0.5, 0.75, 1$) (normal incidence). As seen, 2 strips have resonance frequencies for all values of the fractional orders which is investigated in this article. There exists an analytical expression to find the resonant frequency for such a quasi-resonator when the strips have the same dimensions. For the resonant frequency, the analytical expression gives $kl \approx \frac{\pi n}{2}$ ($n = 1, 2, 3, ...$) [19]. For the first resonance ($n = 1$), the value of kl is equal to $kl \approx \frac{\pi}{2}$. For $n = 2$, $kl \approx \pi$. Our results in Total Radar Cross Section by using fractional derivative approach correspond to the similar outcome with analytical results. In Figures 2, 3, and 5, the wavenumber (k) is changed while the widths of the strips ($a_1 = a_2 = a = 1$) are fixed, and they coincide to the half of the distance between the strips ($l = a_1 = a_2 = a$). The resonant values of ka, which in these cases, are equal to kl, are close to the analytical values. The first resonance is at $ka \approx 1.9$, and the second one is at $ka \approx 3.4$. The deviation from analytical values is because the analytical formulation is derived for the case of the strip which has much larger width than the wavelength ($a \gg \lambda = \frac{2\pi}{k}$) [19].

Figure 3 shows a family of graphs corresponding to different angles of incidence ($\theta = \frac{\pi}{6}, \frac{\pi}{4}, \frac{\pi}{3}, \frac{\pi}{2}$) at $\alpha = 1$. For $\theta = \frac{\pi}{6}, \frac{\pi}{4}, \frac{\pi}{2}$, the resonances at $ka \approx 1.9$ and $ka \approx 3.4$ are preserved, but for $\theta = \frac{\pi}{3}$, it disappears.

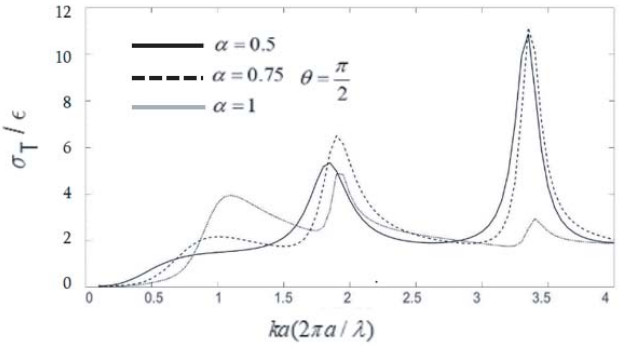

Figure 2. Total Radar Cross Section σ_T when $a = a_1 = a_2 = 1$, $l = 1$, $\theta = \frac{\pi}{2}$ for $\alpha = 0.5$, 0.75, 1.

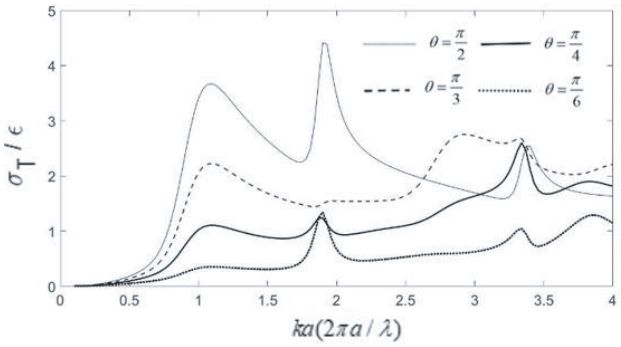

Figure 3. Total Radar Cross Section σ_T when $a = a_1 = a_2 = 1$, $l = 1$, $\alpha = 1$ and $\theta = \frac{\pi}{6}, \frac{\pi}{4}, \frac{\pi}{3}, \frac{\pi}{2}$.

If the distance between the strips is decreased ($l = 0.5$), the first resonance at $ka \approx 1.9$ practically disappears for all angles of incidence because in this case, the widths of the strips are twice of the distance between the strips ($2l$) ($a = a_1 = a_2 = 2l$). The analytical value of the first resonance is no longer at $\frac{\pi}{2}$, but it is at π. Therefore, a resonance appears at $ka \approx 3.4$ which is close to π. This result is shown in Figure 4. It is also considered the case when the fractional order is $\alpha = 0.5$, and then, the corresponding family of graphs is constructed. This is shown in Figure 5. As seen for this case, resonance values are higher. In the previous case (Figure 3 and $\alpha = 1$), first resonance values are up to 5, and the second resonance values are reaching 3. On the other hand, for $\alpha = 0.5$ (Figure 5), the first resonance values are reaching 6, and the second ones are up to 18. Figure 6 represents the total electric field E_z distribution. This field corresponds to the resonant value ($ka_1 = 3.4$). As seen between the strips, there exist high field values, and these high field values correspond to standing wave. Figure 7 gives the total field E_z distribution at the first resonance, ($ka_1 = 1.9$). The field maximum in Figure 7 is higher than the field maximum in Figure 6 (approximately 6 versus 4) as expected from Figure 3. The amplitudes of the total electric fields are given for different configurations in Figures 6–12.

Figure 8 shows the total electric field E_z distribution at a non-resonant frequency ($ka_1 = 1.5$). For this case, high field values are not observed between the strips. After that, the total electric field E_z distribution for intermediate fractional orders is considered. Figure 9 shows the total electric field E_z distribution at the resonance frequency when $\alpha = 0.5$. The field maximum is 9 which is higher than that in the case of Figure 6. Figure 10 shows the total electric field E_z distribution for $\alpha = 0.75$. In this case, the field maximum reaches 10.

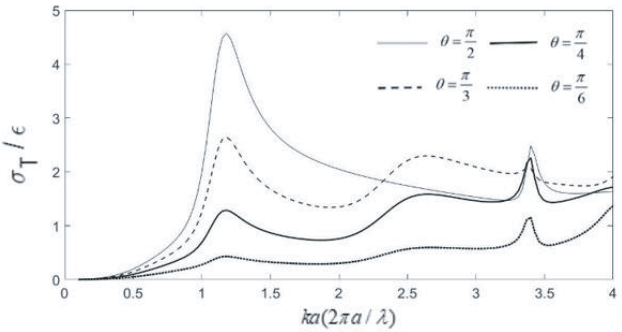

Figure 4. Total Radar Cross Section σ_T when $a = a_1 = a_2 = 1$, $l = 0.5$, $\alpha = 1$ and $\theta = \frac{\pi}{6}, \frac{\pi}{4}, \frac{\pi}{3}, \frac{\pi}{2}$.

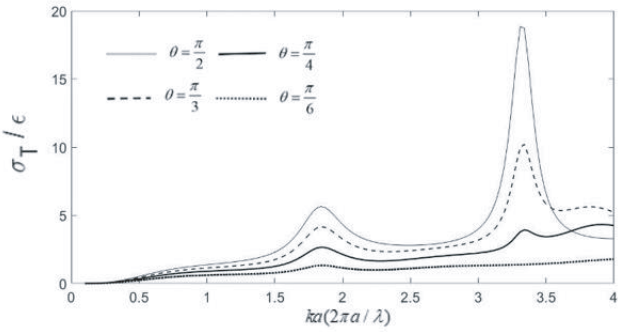

Figure 5. Total Radar Cross Section σ_T when $a = a_1 = a_2 = 1$, $l = 1$, $\alpha = 0.5$ and $\theta = \frac{\pi}{6}, \frac{\pi}{4}, \frac{\pi}{3}, \frac{\pi}{2}$.

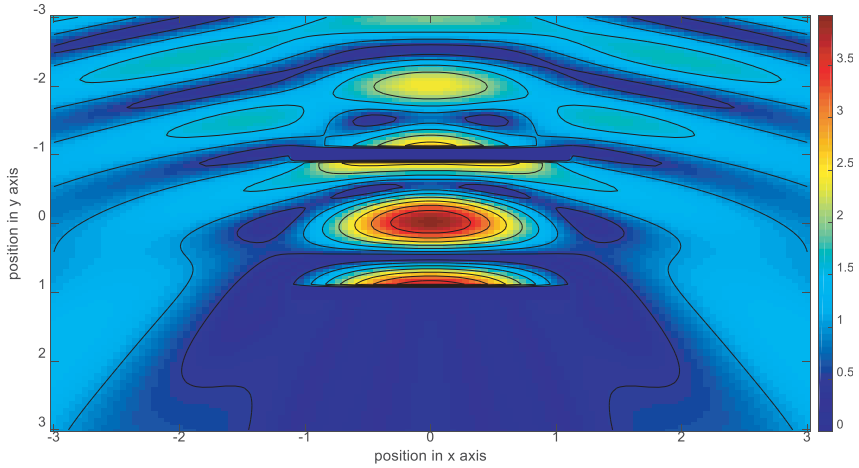

Figure 6. Total electric field E_z, $a_1 = a_2 = 1$, $l = 1$, $\alpha = 1$, $ka_1 = 3.4$, $\theta = \frac{\pi}{2}$.

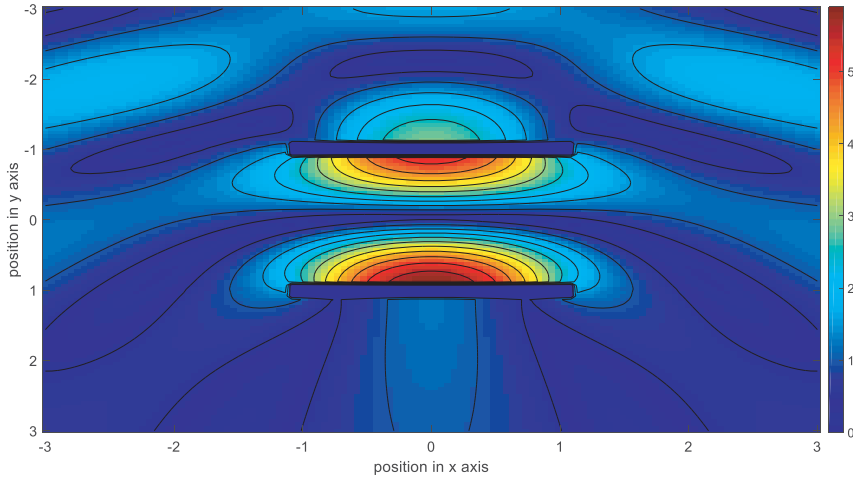

Figure 7. Total electric field E_z, $a_1 = a_2 = 1$, $l = 1$, $\alpha = 1$, $ka_1 = 1.9$, $\theta = \frac{\pi}{2}$.

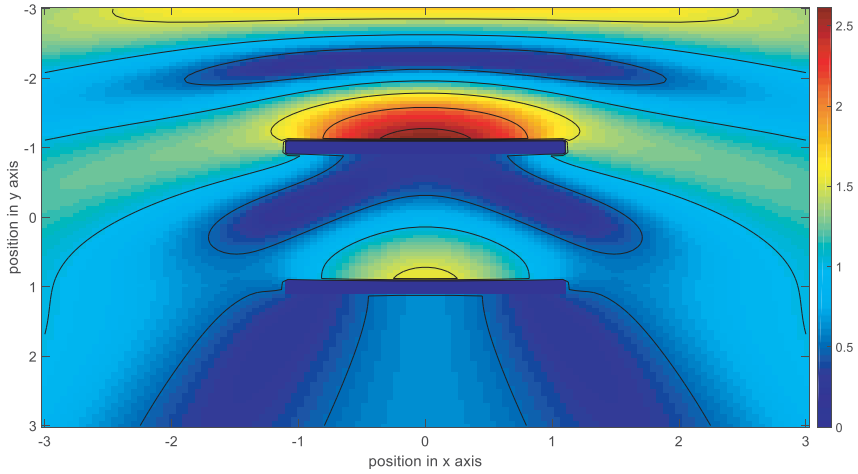

Figure 8. Total field E_z, $a_1 = a_2 = 1$, $l = 1$, $\alpha = 1$, $ka_1 = 1.5$, $\theta = \frac{\pi}{2}$.

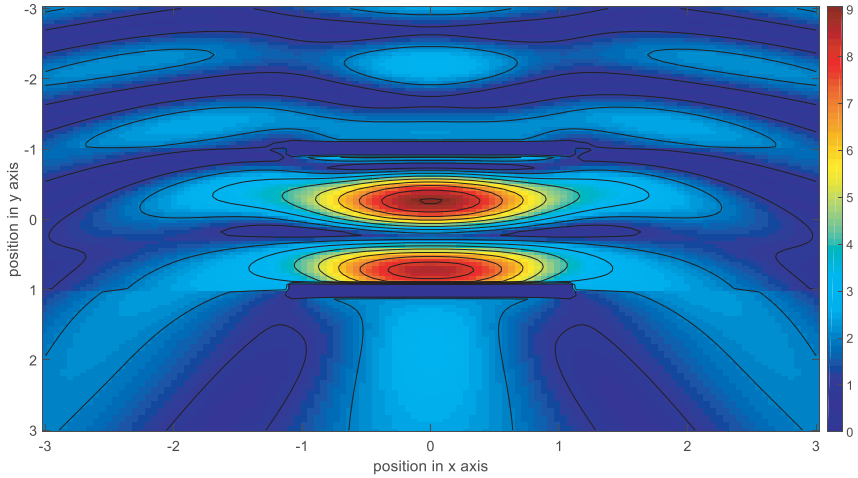

Figure 9. Total electric field E_z, $a_1 = a_2 = 1$, $l = 1$, $\alpha = 0.5$, $ka_1 = 3.4$, $\theta = \frac{\pi}{2}$.

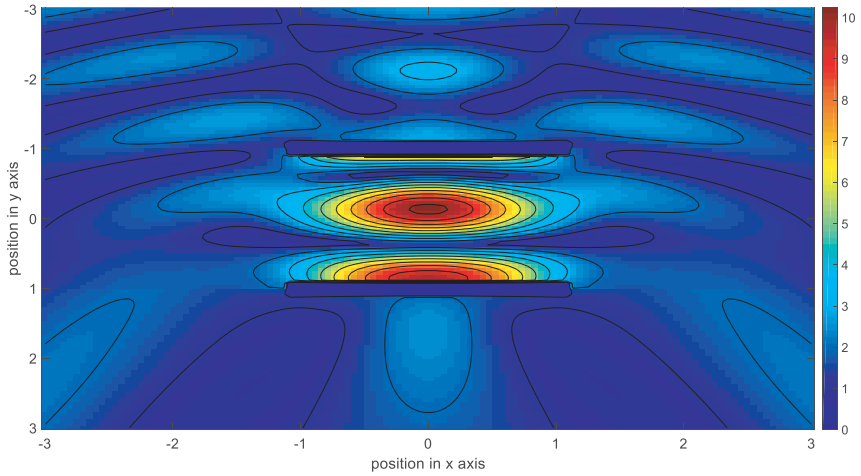

Figure 10. Total electric field E_z, $a_1 = a_2 = 1$, $l = 1$, $\alpha = 0.75$, $ka_1 = 3.4$, $\theta = \frac{\pi}{2}$.

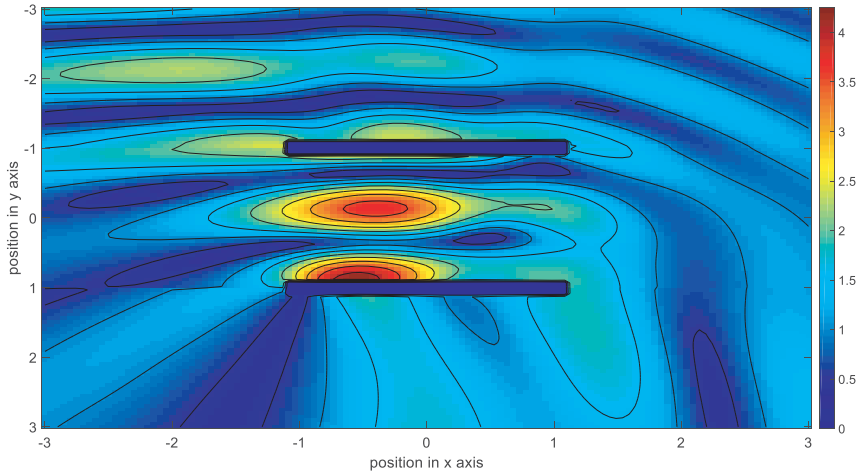

Figure 11. Total electric field E_z, $a_1 = a_2 = 1$, $l = 1$, $\alpha = 0.75$, $ka_1 = 3.4$, $\theta = \frac{\pi}{3}$.

Figure 11 shows the result for the incidence angle $\theta = \frac{\pi}{3}$ instead of $\theta = \frac{\pi}{2}$. As seen, in this case, there exists a resonant field between the strips, but it has a smaller amplitude with respect to the normal incidence case as given in Figure 10 (the maximum amplitude is 4 versus 10). When the incident angle is changed and taken as $\theta = \frac{\pi}{4}$, the results are as given in Figure 12.

For this case, the resonance disappears. The high field values and standing waves between the strips do not exist.

Now, the investigation is done when the strip's dimensions are different: $a_1 = 3$ and $a_2 = 4$.

Figure 13 shows the Total Radar Cross Section dependence on $\epsilon = ka$. As seen, high resonances are observed at $ka_1 \approx 4.8$ and 9.6. The corresponding wavenumber values (k) are $k \approx 1.6$ and $k \approx 3.2$, respectively. Because the half of the distance between the strips (l) is equal to 1, the corresponding values of kl are $kl = 1.6$ and $kl = 3.2$, respectively. This means that by increasing the dimensions of the strips, the resonance frequencies approach analytical values given in the formula $kl \approx \frac{\pi n}{2}$ $(n = 1, 2, ...)$ compared to Figure 2 [19]. The Maximum value of Total Radar Cross Section value reaches 60 at the second resonance $ka_1 = 9.6$ and the fractional order $\alpha = 0.25$. If the incidence angle is taken as $\theta = \frac{\pi}{4}$, the resonance maximum is shifted, broadened, and decreased. This is seen in Figure 14.

After the investigation of TRCS, the total electric field E_z distributions at the resonance frequencies are shown. Figure 15 shows the total electric field E_z distribution at the second resonance. The field maximum is now more than 70. In Figures 15–18, the amplitudes of the total electric fields are given

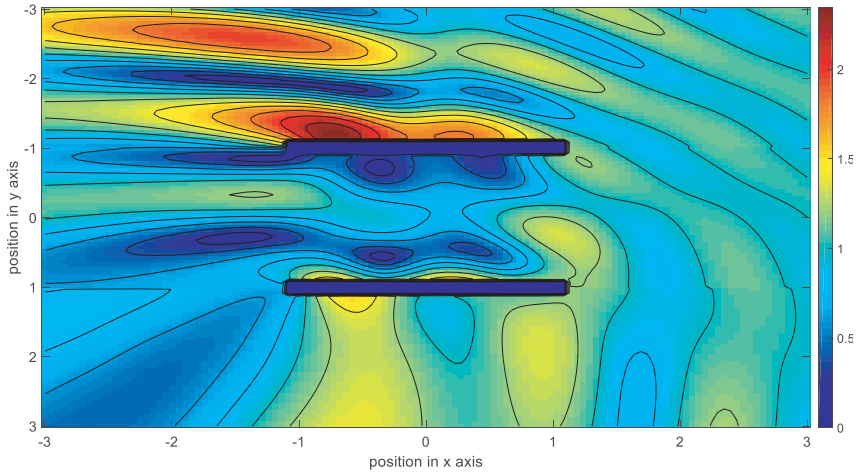

Figure 12. Total field E_z, $a_1 = a_2 = 1$, $l = 1$, $\alpha = 0.75$, $ka_1 = 3.4$, $\theta = \frac{\pi}{4}$.

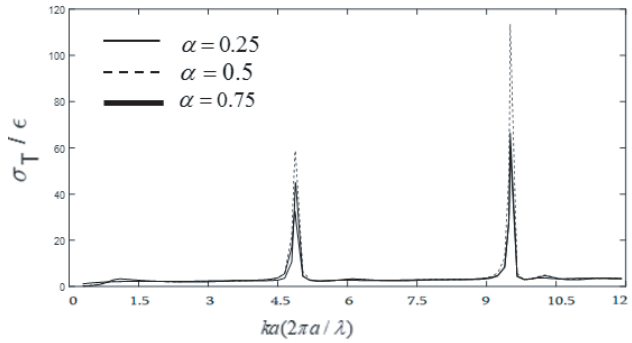

Figure 13. Total Radar Cross Section σ_T when $a = a_1 = 3$, $a_2 = 4$, $l = 1$, $\theta = \frac{\pi}{2}$.

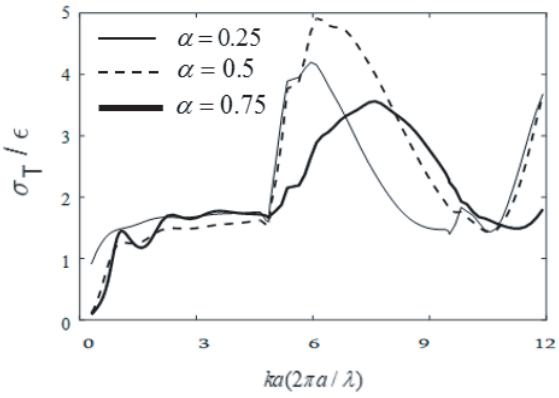

Figure 14. Total Radar Cross Section σ_T when $a = a_1 = 3$, $a_2 = 4$, $l = 1$, $\theta = \frac{\pi}{4}$.

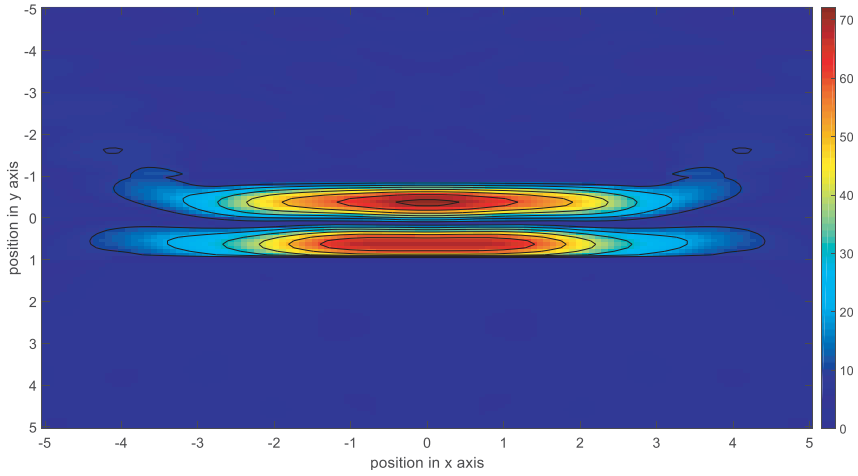

Figure 15. Total field E_z, $a_1 = 3$, $a_2 = 4$, $l = 1$, $\alpha = 0.25$, $ka_1 = 9.5$, $\theta = \frac{\pi}{2}$.

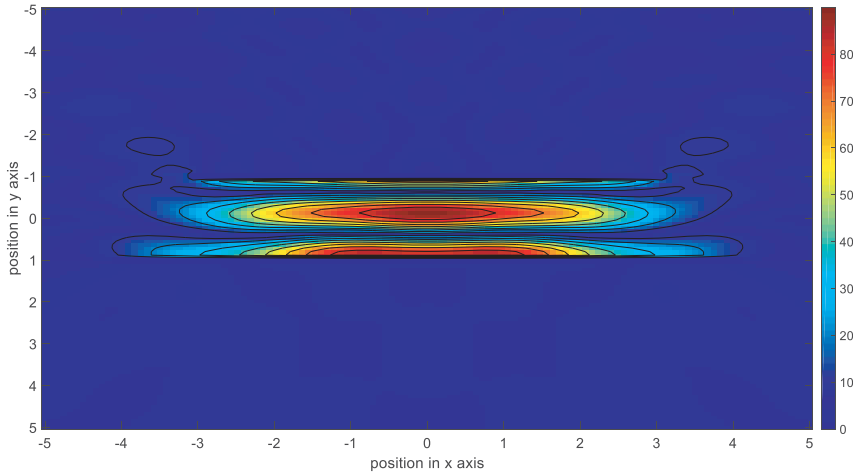

Figure 16. Total electric field E_z, $a_1 = 3$, $a_2 = 4$, $l = 1$, $\alpha = 0.75$, $ka_1 = 9.5$, $\theta = \frac{\pi}{2}$.

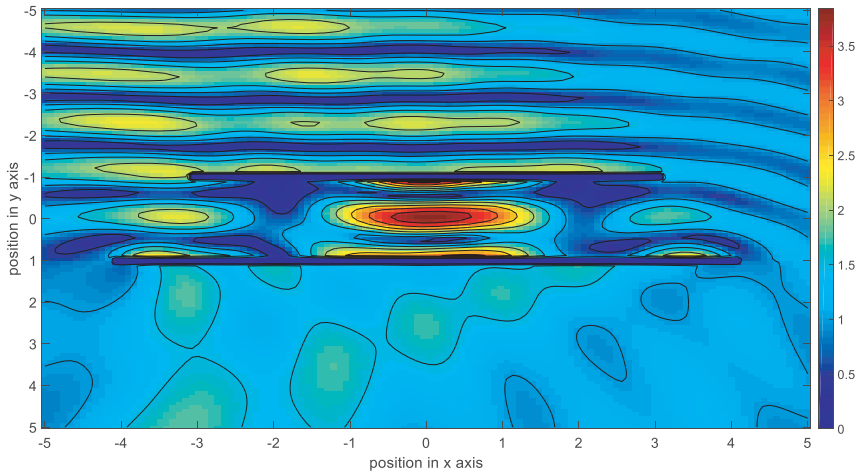

Figure 17. Total electric field E_z, $a_1 = 3$, $a_2 = 4$, $l = 1$, $\alpha = 0.75$, $ka_1 = 9$, $\theta = \frac{\pi}{3}$.

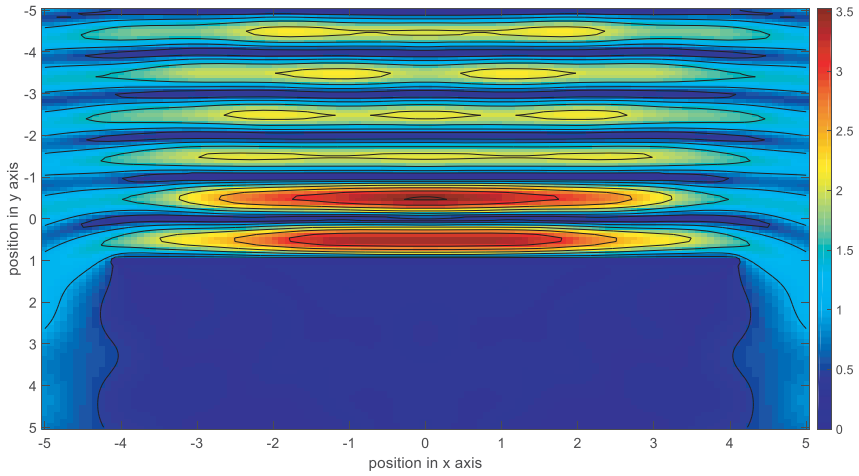

Figure 18. Total electric field E_z, $a_1 = 3$, $a_2 = 4$, $l = 1$, $\alpha = 0.01$, $ka_1 = 9.5$, $\theta = \frac{\pi}{2}$.

for different configurations.

Now, the total electric field E_z distribution is calculated at $\alpha = 0.75$ and compared to Figure 10. The corresponding total field E_z distribution is given in Figure 16.

The total electric field E_z distribution on this figure is similar to Figure 10. The only difference is the higher field amplitudes in this case. In Figure 10, the maximum amplitude is approximately 10. On the other hand, in Figure 16, the maximum amplitude is approximately 90.

If the incidence angle is changed and taken as $\theta = \frac{\pi}{3}$, the total electric field E_z distribution will get the next form which is shown in Figure 17.

As seen, there is still a resonance, but the amplitude of the field between the strips is much smaller, and it is approximately 4. By decreasing the incidence angle, the resonance becomes weaker.

Figure 18 represents the total electric field E_z distribution for the fractional order $\alpha = 0.01$. This is very close to the perfect electric conductor. The maximum field value is 3.5 which is smaller than $\alpha = 0.25$ and $\alpha = 0.75$ cases considered above.

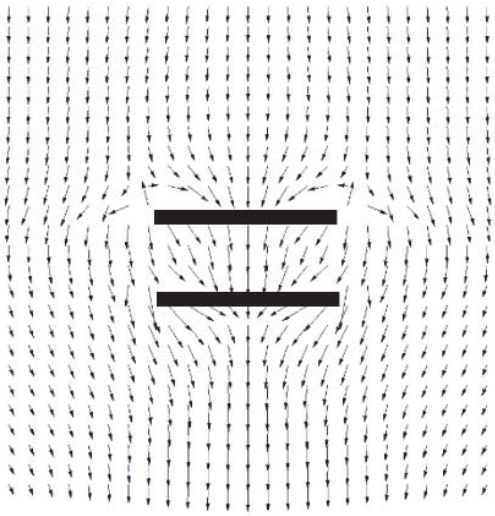

Figure 19. Poynting vector distribution $a_1 = 1$, $a_2 = 1$, $l = 0.5$, $\alpha = 1$, $ka_1 = 1$, $\theta = \frac{\pi}{2}$.

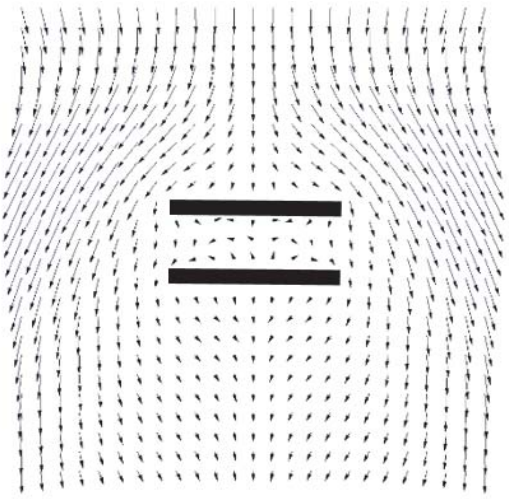

Figure 20. Poynting vector distribution $a_1 = 1$, $a_2 = 1$, $l = 0.5$, $\alpha = 0.01$, $ka_1 = 1$, $\theta = \frac{\pi}{2}$.

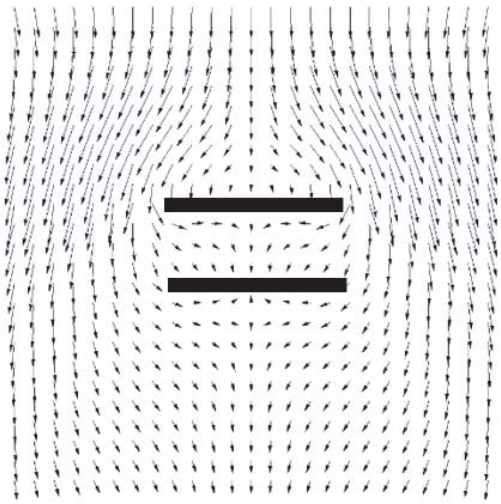

Figure 21. Poynting vector distribution $a_1 = 1$, $a_2 = 1$, $l = 0.5$, $\alpha = 0.5$, $ka_1 = 1$, $\theta = \frac{\pi}{2}$.

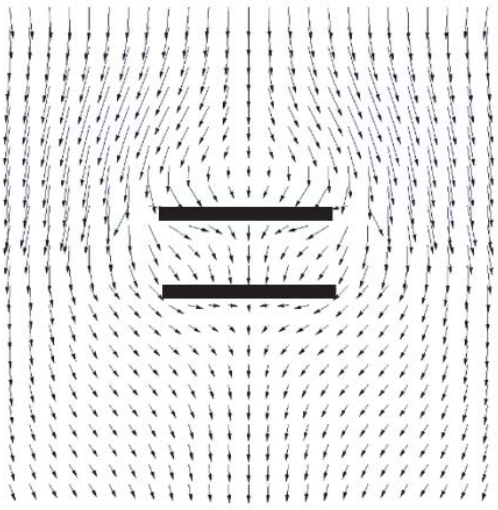

Figure 22. Poynting vector distribution $a_1 = 1$, $a_2 = 1$, $l = 0.5$, $\alpha = 0.75$, $ka_1 = 1$, $\theta = \frac{\pi}{2}$.

Distribution of the Poynting vector given in Eq. (13) is also calculated for different cases. Figure 19 and Figure 20 show the Poynting vector distribution for $\alpha = 1$ and $\alpha = 0.01$, respectively. In the case of Figure 19, diffraction problem corresponds to the PMC case, and the energy penetrates through the strips. On the other hand, Figure 20 stands for PEC case at a non-resonant case ($ka_1 = 1$), so energy flows around the strips and could not penetrate between the strips which creates a shadow region. In other words, in the region between the strips, the Poynting vectors have smaller length.

Figure 21 and Figure 22 show the Poynting vector distribution for $\alpha = 0.5$ and $\alpha = 0.75$, respectively. In Figure 21, the energy goes around the first strip but penetrates through the second strip from both sides. In the case of Figure 22, it is close to PMC due to having fractional order $\alpha = 0.75$, so the flow of the energy is similar to Figure 19.

The Poynting vector distribution is also calculated when strip dimensions and the distance between them are different. Figure 23 and Figure 24 show the Poynting vector distribution when $a_1 = 3$, $a_2 = 4$ for $\alpha = 1$ and $\alpha = 0.01$, respectively. In Figures 23 and 24, it is seen that the energy cannot penetrate between the strips.

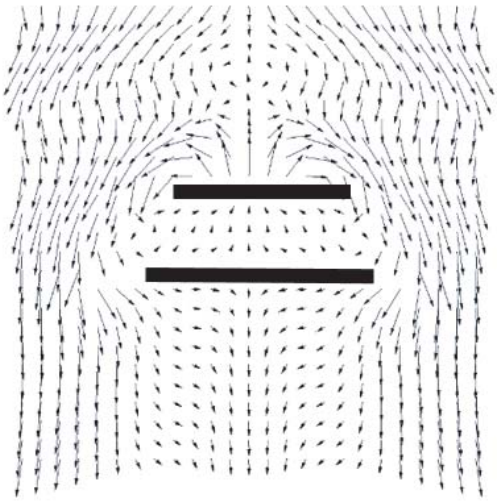

Figure 23. Poynting vector distribution $a_1 = 3$, $a_2 = 4$, $l = 1$, $\alpha = 1$, $ka_1 = 3$, $\theta = \frac{\pi}{2}$.

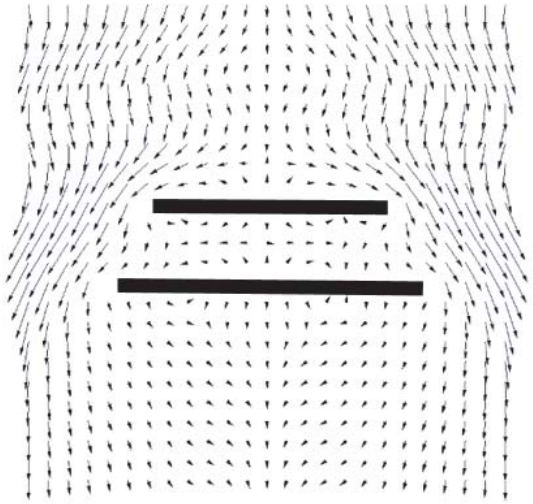

Figure 24. Poynting vector distribution $a_1 = 3$, $a_2 = 4$, $l = 1$, $\alpha = 0.01$, $ka_1 = 3$, $\theta = \frac{\pi}{2}$.

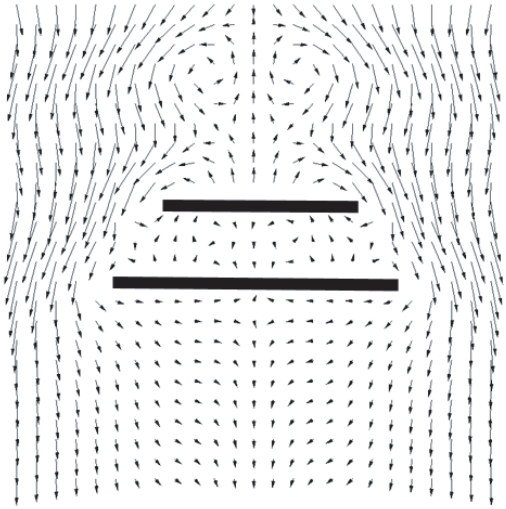

Figure 25. Poynting vector distribution $a_1 = 3$, $a_2 = 4$, $l = 1$, $\alpha = 0.5$, $ka_1 = 3$, $\theta = \frac{\pi}{2}$.

Finally, Figure 25 shows the Poynting vector distribution when $a_1 = 3$, $a_2 = 4$ for $\alpha = 0.5$. Here, vortexes are seen on the upper part.

4. CONCLUSION

In this article, a new mathematical method for the solution of the diffraction problem by the two axisymmetric strips with different widths and fractional boundary conditions is considered. The formulation for plane wave diffraction by the double strips with different sizes is done, and for the FO $\alpha = 0.5$ case, an analytical expression is found. Numerical experiments are conducted for different dimensions of the strips, and Total Radar Cross Section frequency characteristics show that for fractional order between 0 and 1, the resonance peaks are increased, and we get a resonator with higher values of Total Radar Cross Section. The total electric field E_z distribution confirms the existence of high field values between the plates.

ACKNOWLEDGMENT

The authors of this article would like to express the gratitude to Prof. Dr. Nader Engheta and Prof. Dr. Ertuğrul Karaçuha for their useful discussions.

REFERENCES

1. Engheta, N., "Use of fractional integration to propose some "fractional" solutions for the scalar Helmholtz equation," *Progress In Electromagnetics Research*, Vol. 12, 107–132, 1996.
2. Engheta, N., "Fractional curl operator in electromagnetic," *Microwave and Optical Technology Letters*, Vol. 17, No. 2, 86–91, 1998.
3. Engheta, N., "Phase and amplitude of fractional-order intermediate wave," *Microwave and Optical Technology Letters*, Vol. 21, No. 5, 338–343, 1999.
4. Engheta, N., *Fractional Paradigm in Electromagnetic Theory*, Frontiers in Electromagnetics, D. H. Werner and R. Mittra (editors), IEEE Press, 2000.
5. Veliev, E. I. and N. Engheta, "Generalization of Green's theorem with fractional differ integration," *2003 IEEE AP-S International Symposium & USNC/URSI National Radio Science Meeting*, 2003.
6. Veliev, E. I. and M. V. Ivakhnychenko, "Fractional curl operator in radiation problems," *Proceedings of MMET*, 231–233, Dniepropetrovsk, 2004, doi: 10.1109/MMET.2004.1396991.
7. Ivakhnychenko, M. V., E. I. Veliev, and T. M. Ahmedov, "Scattering properties of the strip with fractional boundary conditions and comparison with the impedance strip," *Progress In Electromagnetics Research C*, Vol. 2, 189–205, 2008.
8. Veliev, E. I., T. M. Ahmedov, and M. V. Ivakhnychenko, *Fractional Operators Approach and Fractional Boundary Conditions*, Electromagnetic Waves, Vitaliy Zhurbenko (editor), IntechOpen, 2011, doi: 10.5772/16300.
9. Veliev, E. I., M. V. Ivakhnychenko, and T. M. Ahmedov, "Fractional boundary conditions in plane waves diffraction on a strip," *Progress In Electromagnetics Research*, Vol. 79, 443–462, 2008.
10. Veliev, E. I., K. Karacuha, E. Karacuha, and O. Dur, "The use of the fractional derivatives approach to solve the problem of diffraction of a cylindrical wave on an impedance strip," *Progress In Electromagnetics Research Letters*, Vol. 77, 19–25, 2018.
11. Veliev, E. I., K. Karacuha, and E. Karacuha, "Scattering of a cylindrical wave from an impedance strip by using the method of fractional derivatives," *XXIIIrd International Seminar/Workshop on Direct and Inverse Problems of Electromagnetic and Acoustic Wave Theory (DIPED)*, 2018, doi: 10.1109/DIPED.2018.8543322.
12. Hussain, A. and Q. A. Naqvi, "Fractional curl operator in chiral medium and fractional non-symmetric transmission line," *Progress In Electromagnetics Research*, Vol. 59, 199–213, 2006.
13. Hussain, A., S. Ishfaq, and Q. A. Naqvi, "Fractional curl operator and fractional waveguides," *Progress In Electromagnetics Research*, Vol. 63, 319–335, 2006.

14. Tarasov, V. E., *Fractional Dynamics: Applications of Fractional Calculus to Dynamics of Particles, Fields and Media*, Springer Science & Business Media, 2011, doi: 10.1007/978-3-642-14003-7.
15. Tarasov, V. E., "Fractional vector calculus and fractional Maxwell's equations," *Annals of Physics*, Vol. 323, 2756–2778, 2008, doi: 10.1016/j.aop.2008.04.005.
16. Samko, S. G., A. A. Kilbas, and O. I. Marichev, *Fractional Integrals and Derivatives, Theoryand Applications*, Gordon and Breach Science Publ., Langhorne, 1993.
17. Honl, H., A. Maue, and K. Westpfahl, *Theorie der Beugung*, Springer-Verlag, Berlin, 1961.
18. Ishimaru, A., *Electromagnetic Wave Propagation, Radiation, and Scattering: From Fundamentals to Applications*, John Wiley & Sons, 2017.
19. Balanis, C. A., *Advanced Engineering Electromagnetics*, John Wiley & Sons Inc., New York, 1989.